Engineering Structures 366 (2026) 123282

Contents lists available at ScienceDirect

Engineering Structures

journal homepage: www.elsevier.com/locate/engstruct

Physics-informed probabilistic neural network for reliable condition assessment and failure prognosis of substructures in floating offshore wind turbines

Zifei Xu [a,b,c,*]

[a] School of Power and Energy Engineering & Mechanical Engineering, University of Shanghai for Science and Technology, Shanghai, China
[b] Department of Civil and Environmental Engineering, University of Liverpool, Liverpool, UK
[c] Liverpool Logistics Offshore and Marine Research Institute, Liverpool John Moores University, Liverpool, UK

ARTICLE INFO

Keywords:
Prognostics and health management
Floating offshore wind turbine
Uncertainty quantification
Physics-informed Machine Learning
Lifecycle Reliability

ABSTRACT

The structural integrity of substructures in Floating Offshore Wind Turbine (FOWTs) is critical importance and efficient and reliable health condition assessment methods are essential to ensure their long-term reliability and safety. Modern intelligent prognostic approaches based on deep neural networks are generally developed by learning the mapping between theoretical health condition with the monitoring observations. However, their performance can deteriorate significantly when failure data are limited or unavailable. To address these challenges, this study proposes a reliable intelligent prognostic framework capable of predicting failures even in the absence of direct failure observations. The proposed framework consists of three main modules: (i) a robust health indicator construction module for extracting representative degradation information from monitoring data; (ii) a Physics-Informed Dual Decoder prognostic module, which incorporates physics-informed inductive bias to constrain latent fatigue-evolution dynamics and predict future health states; and (iii) a reliability assessment module for quantifying structural reliability based on the prognostic results. The framework's effectiveness is validated through fatigue degradation analysis on three typical FOWT substructures. The results show that, as structural fatigue degradation progresses, degradation-related dynamic response changes can be effectively captured by the proposed TDA-VMD-based health indicator construction method, leading to more robust health assessment features. Furthermore, by introducing physics-informed inductive bias to constrain the latent dynamics of fatigue evolution, the proposed PIDualDecoder model enables more physically consistent and reliable fatigue prognosis, particularly for long-term prediction. These improved prognosis results further provide more confident support for reliability assessment, thereby contributing to safer and more cost-effective operation and maintenance of FOWTs.

1. Introduction

Rapid advancements in floating offshore wind technology have made Floating Offshore Wind Turbines (FOWTs) a promising clean energy solution for the future, as highlighted by recent studies [1,2], which underscore the potential of these technologies for sustainable energy generation. FOWTs are becoming increasingly efficient and reliable. However, from an economic perspective, their operation and maintenance (O&M) costs remain significantly higher than those of onshore and bottom-fixed offshore wind turbines (WTs). This is primarily due to their deployment in harsh marine environments including icing with limited accessibility, which leads to increased installation, monitoring, and maintenance costs [3,4]. As a result, it becomes particularly challenging to manage site operations effectively, including continuous monitoring and timely maintenance scheduling [5]. In the event of component failures, this limited accessibility may result in longer downtimes for FOWTs compared to their onshore and fixed-bottom counterparts [6]. Condition Monitoring Systems (CMS), which provide an effective means of assessing the health status of FOWTs, can be used to detect early-stage anomalies and predict the remaining useful life of critical components [7]. These capabilities help to prevent catastrophic failures and reduce downtime, ultimately achieving cost savings in O&M [8]. However, FOWTs face additional challenges, with one of the

* Corresponding author at: School of Power and Energy Engineering & Mechanical Engineering, University of Shanghai for Science and Technology, Shanghai, China.

E-mail addresses: zxu@usst.edu.cn, zifei.xu@liverpool.ac.uk, z.xu@ljmu.ac.uk.

https://doi.org/10.1016/j.engstruct.2026.123282
Received 21 August 2025; Received in revised form 6 June 2026; Accepted 25 June 2026
Available online 6 July 2026

Nomenclature

FOWTs	Floating offshore wind turbines.
O&M	Operation and Maintenance.
WTs	Wind turbines.
CMS	Condition monitoring systems.
RUL	Remaining useful life.
PHM	Prognostics and health management.
LSTM	Long short-term memory.
Bi-LSTM	Bidirectional long short-term memory.
GRU	Gated recurrent unit.
AM	Attention mechanism.
CNN	Convolutional neural network.
VMD	Variational mode decomposition.
BNN	Bayesian neural network.
IMF	Intrinsic mode function.
N_c	the total number of cycles.
ML	Machine learning.
DL	Deep learning.
UQ	Uncertainty quantification.
AI	Artificial intelligence.
MAE	Mean absolute error.
6-DOFs	Six Degrees of Freedoms.
SOTA	Several state-of-the-art.
ADMM	Alternating direction method of multipliers.
DI	Degradation indicator.
HI	Health indicator.
KECA	Kernel entropy component analysis.
WOA	Whale optimization algorithm.
NN	Neural network.
RNN	Recurrent neural network.
$N_f(\sigma_{m,i}, \sigma_{\alpha,i})$	the number of cycles to failure.
$\mathrm{Life}_{\mathrm{accelerated}}\|\nu$	estimated run-to-failure life under this condition.
D_{total}	the total damage.
λ	the Lagrangian multiplier.
TN	Penalty factor (VMD parameter).
MC	Transformer network.
TDA-VMD	Task-driven adaptive variational mode decomposition.
TDA-VMD	Task-driven adaptive variational mode decomposition.
NSGA-II	Non-dominated sorting genetic algorithm II.
PIDualDecoder	Physics-informed Dual Decoder framework.
PDE	Partial differential equation.
TLP	Tension leg platform.
RMSE	Root means square error.
BTN	Bayesian transformer network.
PDFs	Probability density functions.
CDFs	Cumulative distribution functions.
EOCs	Environmental and operating conditions.

primary limitations of their sustainability being the high O&M costs. These costs are largely driven by the complex marine environment and dynamic loading conditions, which increase the likelihood of failure in key components such as drivetrains and electrotechnical systems [9]. Although tuned mass dampers (TMDs) can effectively reduce platform vibration, they do not eliminate the progression of structural degradation and fatigue damage under long-term cyclic loading [10]**.** Therefore, advanced health monitoring and prognostic approaches remain essential to ensure the reliability and cost-effectiveness of FOWTs. While key reliability techniques in Prognostics and Health Management (PHM), including anomaly detection, fault diagnosis, and prognosis, have been extensively studied for drivetrains in onshore wind turbines and other electromechanical systems, making them relatively transferable to FOWT applications, the reliability of sub-structures remains underexplored [11]. The sub-structures, however, are critical to the overall safety and operational stability of FOWTs, yet widely adopted reliability techniques for these components are still lacking. Therefore, this research aims to address the PHM challenges associated with the mooring system, a critical sub-structure of FOWTs, by adopting a reliability-oriented approach that focuses on the construction of degradation indicators and the development of effective prognosis techniques.

Quantifying structural damage through degradation indicators (DIs), also referred to as health indicators (HIs), is a critical prerequisite for reliable prognostics. Existing HI construction methods have evolved from traditional feature fusion approaches to physics-informed and data-driven representation learning techniques. Early studies primarily focused on integrating multiple condition-monitoring features to improve degradation quantification. For example, Wang et al. [12] employed Mahalanobis distance to fuse more than ten statistical features and measure deviations from the healthy state, demonstrating that multi-feature fusion can significantly enhance HI robustness. Similarly, He et al. [13] developed an intelligent feature-learning framework capable of automatically identifying failure and maintenance patterns in wind turbines, providing reliable data support for subsequent prognostic and maintenance decision-making tasks. To improve the physical interpretability of HIs, researchers have increasingly incorporated domain knowledge into the indicator construction process. Liu et al. [14] combined Hilbert–Huang transform-based signal decomposition with Spearman's correlation analysis to identify fault-sensitive features, enabling a more physically meaningful assessment of degradation progression and prediction accuracy. More recently, advances in deep learning have enabled automatic extraction of degradation representations directly from raw monitoring data. Xu et al. [15] proposed a Transformer-based encoder–decoder framework that learns latent degradation features without manual feature engineering, while similarity measures were employed to quantify deviations between healthy and degraded conditions. Qiu et al. [16] integrated entropy-weighted kernel entropy component analysis (KECA)-based HI construction, degradation point detection, and a WOA-optimized Attention-BiLSTM network, achieving improved prognostic accuracy, robustness, and computational efficiency.

While constructing a reliable health indicator is critical, it is equally important for prognosis to accurately predict damage progression or estimate the remaining useful life based on that indicator. Use of physical and data-driven models are part of the mainstream processes for developing a prognosticator to estimate the RUL. However, in the present era of industrial big data, the data-driven based health state prediction method is preferred because of recent advances on it as a research topic.

Lu et al. [17] developed an initial data-driven neural network model for predicting wind turbine component failures, focusing on mapping degradation features to failure outcomes. Building on this, Jimenez et al. [18] introduced enhancements to the network architecture to better capture nonlinearity and improve prediction accuracy. Subsequently, Laguna et al. [19] further advanced the approach by incorporating a more comprehensive feature mapping strategy using deep learning techniques. They used a deep learning neural networks (NN) to improve the accuracy of the developed prognostic model by mapping the degradation features. Conversely, ignoring the time dependence between the degradation feature in the study reduces the performance of the NN-based prognosticators. Thus, recurrent neural network (RNN) and its variants including LSTM, Bi-LSTM and GRU are used to develop the prognostic model. Huang et al. [20] developed a prognostic model based on Bi LSTM algorithm. The authors combined sensor-data with operational data to train the prognostic model to improve its prediction accuracy under various operational conditions. Chen et al. [21] proposed an RNN-based approach with attention mechanism (AM) for RUL prediction of machines. The AM was embedded in the approach to capture the most relevant features to improve prediction accuracy. Xu et al. [22] combined the advantages of CNN and LSTM to develop a model to predict the failure of rotating machinery. The model uses less feature weights to predict failure for industrial grade application. A highlight of the prognostic model is its ability to reliably predict the failure. This suggests that a prognostic approach should be established based on accuracy and reliability. For example, Guo et al. [23] and Wang et al. [24] developed hybrid deep learning frameworks that combine feature extraction and degradation modelling to improve prognostic robustness and maintenance decision-making. Their studies highlight the effectiveness of data-driven models in capturing complex degradation patterns without extensive manual feature engineering. To enhance reliability under uncertainty, probabilistic learning methods have attracted considerable attention. Traditional intelligent PHM frameworks based on variational mode decomposition, probabilistic neural networks, and nonlinear dynamic analysis have shown effectiveness in noisy and complex operating environments [25,26]. More recently, Bayesian deep learning approaches have been introduced to explicitly quantify prediction uncertainty. Fang et al. [27] employed Bayesian convolutional neural networks for fault diagnosis under noisy conditions, while Li et al. [28] further improved uncertainty estimation in RUL prediction through a Bayesian neural network combined with a sequential Bayesian boosting strategy. In addition, multi-source information fusion has been explored to improve prognostic accuracy by exploiting complementary degradation information from different monitoring channels [29].

Despite their success, purely data-driven methods often suffer from limited generalisation and reduced interpretability when operating conditions differ from the training environment. To address this limitation, physics-informed learning has recently emerged as a promising direction for RUL prediction. By incorporating degradation mechanisms, governing equations, or physical constraints into the learning process, physics-informed models can improve prediction consistency and reduce dependence on large labelled datasets. For instance, physics-informed data augmentation techniques have been developed to enrich degradation trajectories and enhance prediction performance under limited data conditions [30]. Self-attention assisted physics-informed neural networks have been proposed to integrate temporal dependencies with physical knowledge for more accurate RUL estimation [31]. Furthermore, physics-informed multi-state temporal frequency networks have demonstrated improved capability in capturing degradation evolution across multiple operating states while preserving physical consistency [32].

Challenges arise in both health indicator development and fatigue prognosis modelling. For health indicator construction, damage quantification in FOWTs is particularly difficult because stochastic environmental loads lead to unstable dynamic responses and increased uncertainty in monitoring data.

For fatigue prognosis, conventional data-driven models often rely on direct sequence mapping from historical observations to future damage, without sufficiently incorporating historical degradation estimation and the physical relationship between monitoring responses and fatigue evolution [33]. In addition, deterministic prediction may provide limited reliability when uncertainty is not properly characterized. Therefore, this study aims to establish a reliable prognosis framework for the health assessment and condition monitoring of FOWT substructures by developing a robust health indicator construction approach and a trustworthy fatigue prognosis model with physics-informed learning and uncertainty-aware prediction. The main contributions of this research are as follows:

(i) A health indicator construction method is proposed to reduce uncertainty across monitoring data and provide a basis for damage prediction.

(ii) A neural network framework, termed PIDualDecoder, is developed for fatigue prognosis. The architecture integrates historical estimation into future-state prediction and incorporates a general ODE-based formulation to introduce physics-related inductive bias.

(iii) A reliability analysis module is established based on the prognosis results, forming an integrated pipeline from monitoring data analysis and damage detection to prognosis and reliability assessment. This framework provides decision-support information for structural health monitoring and maintenance management of FOWTs.

The rest of the paper is organized as follows: Section 2 provides an overview of the preliminaries including the backbone of the proposed methods and how to get the simulation dataset. Section 3 presents the proposed methodologies including the TDA-VMD based HI construction and the Prognostic framework. Section 4 introduces the experimental setup and evaluation metrics. Section 5 discusses and analyzes the reliability and superiority of the proposed methods. Finally, Section 6 concludes and summarizes the findings.

2. Preliminaries

2.1. Accelerated fatigue simulation framework

As a key component of FOWT sub-structures, the mooring system, serving as part of the platform's support, plays a critical role in ensuring the overall operational stability of FOWTs. Therefore, the main objective of this study is to quantify the structural degradation of mooring lines through the platform's dynamic responses and estimate the progression of this degradation to achieve effective prognosis. To this end, it is first necessary to obtain the dynamic responses of FOWTs when the mooring lines are at different stages of degradation. Therefore, this subsection introduces a fast simulation approach for structural degradation of FOWTs based on OpenFAST [34].

Generally, Rainflow counting is commonly used to identify complete stress cycles, while S–N curves and Miner's rule are applied to evaluate the accumulated fatigue damage of critical structures [35]. For the critical sub-structures of FOWTs, the moorings are subjected to complex and fluctuating environmental loads including wind, wave, and current interactions. In this study, the time-varying tension response $T(t)$ at the mooring fairlead is used as the load input. Although the available S–N curves are stress-based, the tension signal is converted into an equivalent stress signal using the nominal cross-sectional area A of the mooring line $\sigma(t) = T(t)/A$. This stress time series is then subjected to rainflow cycle counting to identify all effective stress cycles within the time interval T_c. Each extracted cycle is defined by its mean stress $\sigma_{m,i}$ and stress range or amplitude $\sigma_{\alpha,i}$, and the corresponding fatigue damage is calculated using the S–N curve and Miner's rule:

$$D_c = \sum_{i=1}^{N_c} 1/N_f(\sigma_{m,i}, \sigma_{\alpha,i}) \tag{1}$$

Where N_c is the total number of cycles, $N_f(\sigma_{m,i}, \sigma_{\alpha,i})$ represents the number of cycles to failure corresponding to each cycle in the dynamic loading process.

In this study, the fatigue damage is evaluated based on the dynamic tension response at the connection between the platform and the mooring line, which is generally regarded as the most fatigue-critical region due to its exposure to high dynamic loads and structural discontinuities [36]. By estimating the accumulated fatigue damage at this interface, the structural integrity of the entire mooring line is approximated, under the assumption that this location governs the fatigue life of the system. This approach is considered conservative and practical for early-stage design evaluation, where full-length stress analysis along the mooring line is not computationally feasible [37].

In traditional fatigue life estimation approaches, the expected fatigue damage over a full design life T_{design} is calculated by integrating the

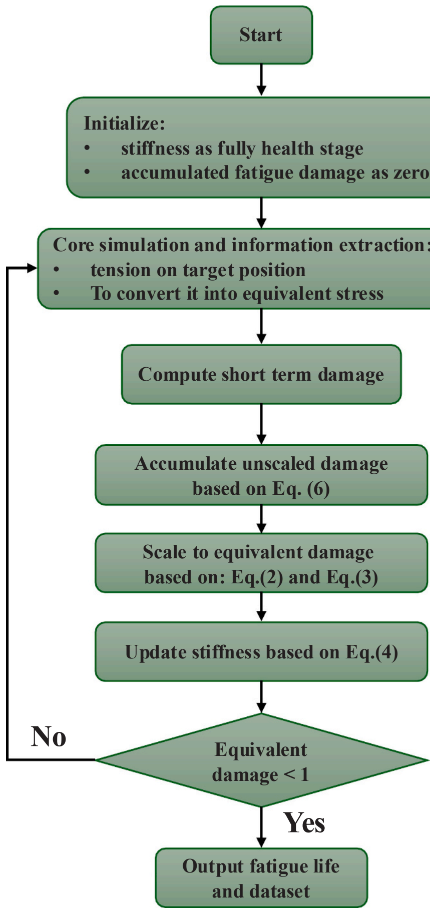

Fig. 1. Fatigue degradation simulation framework.

damage contributions across various operational conditions, weighted by their statistical occurrence probabilities. However, this study aims to investigate the damage accumulation process under a specific wind condition and quantify its impact on structural degradation, with the goal of constructing a health indicator (HI) for fatigue prognosis. To this end, a run-to-failure simulation framework is established in Fig. 1, where the mooring line is subjected to continuous loading at a fixed wind speed v.

The accumulated fatigue damage over a simulation duration T is quantified using the rainflow counting method and Miner's rule. The equivalent fatigue life under this condition, without probabilistic extrapolation, is calculated as:

$$\mathrm{Life}_{\mathrm{accelerated}}|v = T\ /D|v \tag{2}$$

where $D|v$ is the total damage accumulated during simulation time T under wind speed v, and $\mathrm{Life}_{\mathrm{accelerated}}|v$ is the estimated run-to-failure life under this condition.

Since this simulation does not account for the actual statistical distribution of wind speeds throughout the entire design life, a correction factor is introduced to scale the accumulated damage relative to the expected design life $\mathrm{T}_{\mathrm{design}}$. The corrected damage is given by:

$$\mathrm{D}_{\mathrm{corrected}} = \mathrm{D} \bullet \frac{\mathrm{Life}_{\mathrm{accelerated}}|v}{\mathrm{T}_{\mathrm{design}}} \tag{3}$$

.

This corrected damage $\mathrm{D}_{\mathrm{corrected}}$ is then used to track the evolution of structural degradation and to construct a time-dependent HI for fatigue prognosis.

To model the fatigue-induced degradation of structural stiffness, a nonlinear exponential mapping based on a Weibull-type degradation function is adopted [38, 39]. The initial axial stiffness $EA_{initial}$ is assumed to decay as a function of the accumulated fatigue damage D_{total}, following:

$$EA = EA_{initial} \bullet \mathrm{e}^{-(\frac{\mathrm{D}_{total}}{\mu})^{\beta}} \tag{4}$$

Where the total damage D_{total} is updated iteratively after each simulation cycle.

Within each run-to-failure simulation conducted at a fixed wind speed. μ and β are the scale and shape parameters of the Weibull-type degradation function, respectively. Specifically, μ controls the damage level at which significant degradation begins, while β defines the rate of stiffness decay with increasing accumulated damage. The total damage is updated:

$$\mathrm{D}_{total} \leftarrow \mathrm{D}_{total} + \mathrm{D}_{local} \tag{6}$$

Where D_{local} refers to the corrected fatigue damage increment obtained from the current simulation interval. Once $\mathrm{D}_{total} \geq 1$ the structure is considered to have reached fatigue failure.

2.2. Variational mode decomposition

In real engineering applications, signals such as vibration, temperature, and current are often non-stationary in nature. These signals contain crucial information related to the damage evolution and structural health status. Therefore, accurate signal decomposition plays a vital role in the preprocessing stage of intelligent prognostics [40].

The Variational Mode Decomposition (VMD) algorithm decomposes a complex signal into multiple sub-signals (Intrinsic Mode Functions, IMF) with finite bandwidths [41]. Each IMF is treated as an amplitude-modulated and frequency-modulated (AM-FM) signal, defined as:

$$u_k(t) = A_k(t)\cos(\varphi_k(t)) \tag{7}$$

where $\varphi_k(t)$ is the instantaneous phase of the k^{th} IMF, and $A_k(t)$ is the instantaneous amplitude.

To obtain IMFs with compact bandwidths, VMD formulates a constrained variational problem, where the bandwidth of each mode is measured by the squared L2-norm of the gradient of its analytic signal after Hilbert transform and baseband demodulation. The optimization objective is given by:

$$\begin{cases} \& \min\limits_{\{u_k\}\{\omega_k\}} \left\{ \sum_{k=1}^{K} \left\| \partial_t \left[\left(\delta(t) + \frac{j}{\pi t} \right) \times u_k(t) \right] e^{-j\omega_k t} \right\|_2^2 \right\} \\ \qquad \& \mathrm{s.t.} \sum_{k=1}^{K} u_k = f \end{cases} \tag{8}$$

where $\{u_k\} = \{u_1, u_2, u_3 \cdots, u_K\}$, are the K modes to be solved, and $\{\omega_k\} = \{\omega_1, \omega_2, \omega_3 \cdots, \omega_K\}$ are their corresponding center frequencies. The Dirac delta function is denoted by $\partial_t(\cdot)$, and j is the imaginary unit.

To solve the above constrained optimization problem, the augmented Lagrangian multiplier method is used, resulting in the following Lagrangian function:

$$\begin{aligned} L(\{u_k\}, \{\omega_k\}, \lambda) = \alpha \sum_{k=1}^{K} \left\| \partial_t \left[\left(\delta(t) + \frac{j}{\pi t} \right) \times u_k(t) \right] e^{-j\omega_k t} \right\|_2^2 + \Bigg\| f(t) \\ - \sum_{k=1}^{K} u_k(t) \Bigg\|_2^2 + \langle \lambda(t), f(t) - \sum_{k=1}^{K} u_k(t) \rangle \end{aligned} \tag{9}$$

where α is the penalty parameter, and λ is the Lagrangian multiplier. Eq. (8) is solved iteratively using the Alternate Direction Method of Multipliers (ADMM), and the IMF updates in the frequency domain are given

Table 1
Computational steps of the VMD algorithm.

Step	Execution Details
1	Initialize$\{u_k^1\}$、$\{\omega_k^1\}$、λ^1 and n to zero
2	Set iteration counter $n = n + 1$ and start loop
3	Update u_k and ω_k using Eq. (10) and Eq. (11)
4	Increment $k = k + 1$, repeat Step 3 until $k = K$
5	Update Lagrange multiplierλ using Eq. (12)
6	Check convergence using Eq. (13)

as:

$$\widehat{u}_k^{n+1}(\omega) = \frac{\widehat{f}(\omega) - \sum_{i=1}^{k-1}\widehat{u}_i^{n+1}(\omega) - \sum_{i=k+1}^{K}\widehat{u}_i^{n}(\omega) + \frac{\widehat{\lambda_i(\omega)}}{2}}{1 + 2\alpha(\omega - \omega_k^n)^2} \tag{10}$$

$$\omega_k^{n+1} = \frac{\int_0^\infty \omega\left|\widehat{u}_k^{n+1}(\omega)\right|^2 d\omega}{\int_0^\infty \left|\widehat{u}_k^{n+1}(\omega)\right|^2 d\omega} \tag{11}$$

$$\widehat{\lambda}^{n+1}(\omega) = \widehat{\lambda}^{n}(\omega) + \tau\left(\widehat{f}(\omega) - \sum_{k=1}^{K}\widehat{u}_k^{n+1}(\omega)\right) \tag{12}$$

where τ is the dual ascent step size. The iteration process stops when the following convergence condition is satisfied:

$$\sum_{k=1}^{K}\left(\left\|\widehat{u}_k^{n+1}(\omega) - \widehat{u}_k^{n}(\omega)\right\|_2^2 \Big/ \left\|\widehat{u}_k^{n}(\omega)\right\|_2^2\right) < \varepsilon \tag{13}$$

.

In this work, the convergence threshold is set to $\varepsilon = 10^{-6}$.

The computational steps of the VMD algorithm are summarized in Table 1.

2.3. Prognosis problem definition

Generally, both remaining useful life prediction and fatigue damage prediction can be formulated within the same statistical learning framework, where the degradation-related target is inferred and forecast from multivariate monitoring signals [42, 43]. Let a variable-length sample be denoted by $\mathscr{D} = \{(\mathbb{x}_t, \mathbb{y}_t)\}_{t=1}^{T}$, where $\mathbf{x}_t \in \Re^{d_x}$is the multivariate observation at time step t, and $\mathbb{y}_t \in \Re$ is the target variable. Given an observed prefix of length k and a forecasting horizon of length h, we define the total prediction length as $S = k + h$, with input sequence $\mathbb{X}_{1:k} = (\mathbb{x}_1, \ldots, \mathbb{x}_k)$and target sequence $\mathbb{Y}_{1:S} = (\mathbb{y}_1, \ldots, \mathbb{y}_S)$. The learning objective is to estimate a conditional distribution$p_\theta(\mathbb{Y}_{1:S}|\mathbb{X}_{1:k})$, where $\theta \in \Theta$ denotes the model parameters. In this work, the conditional distribution is specified as a stepwise heteroscedastic Gaussian model [44]:

$$p_\theta(\mathbb{Y}_{1:S}|\mathbb{X}_{1:k}) = \prod_{t=1}^{S}\mathscr{N}\left(\mathbb{y}_t; \mu_{\theta,t}(\mathbb{X}_{1:k}), \sigma_{\theta,t}^2(\mathbb{Y}_{1:S})\right) \tag{14}$$

.

Accordingly, the model parameters are learned by maximizing the conditional likelihood of the target sequence given the observed input sequence: $\theta^* = -\underset{\theta}{\operatorname{argmax}} p_\theta(\mathbb{Y}_{1:S}|\mathbb{X}_{1:k})$. Equivalently, the training objective can be formulated as minimizing the negative log-likelihood (NLL):

$$\mathscr{L}_{\mathrm{NLL}}(\theta) = -\log p_\theta(\mathbb{Y}_{1:S}|\mathbb{X}_{1:k}) \tag{15}$$

.

By substituting Eq. (14) and Eq. (15), the loss becomes:

$$\mathscr{L}_{\mathrm{NLL}}(\theta) = -\sum_{t=1}^{S}\log\mathscr{N}\left(\mathbb{y}_t; \mu_{\theta,t}(\mathbb{X}_{1:k}), \sigma_{\theta,t}^2(\mathbb{X}_{1:k})\right) \tag{16}$$

.

Using the logarithmic form of the Gaussian density, the loss can be further written as:

$$\mathscr{L}_{\mathrm{NLL}}(\theta) = \frac{1}{2}\sum_{t=1}^{S}\left[\log(2\pi\sigma_{\theta,t}^2(\mathbb{X}_{1:k})) + \frac{(\mathbb{y}_t - \mu_{\theta,t}(\mathbb{X}_{1:k}))^2}{\sigma_{\theta,t}^2(\mathbb{X}_{1:k})}\right] \tag{17}$$

.

2.4. Bayesian approximation via Monte Carlo Dropout

Monte Carlo dropout is adopted as an approximate Bayesian inference strategy [45]. During prediction, dropout remains active to generate stochastic outputs for uncertainty estimation. Let ω denote the network parameters and $\mathscr{D}$the training data. In Bayesian learning, the posterior over weights is formally given by:

$$p(\omega|\mathscr{D}) = \frac{p(\mathscr{D}|\omega)p(\omega)}{p(\mathscr{D})} \tag{18}$$

.

Dropout is used to approximate the posterior predictive distribution by randomly sampling subnetworks through stochastic dropout masks. For an input x, the predictive distribution is approximated as:

$$p(\mathbb{y}|\mathbb{x}, \mathscr{D}) \approx \int p(\mathbb{y}|\mathbb{x}, \omega)\, q(\omega)\, d\omega \tag{19}$$

where $q(\omega)$denotes the dropout-induced approximate posterior. In practice, this distribution is estimated through Mstochastic forward passes with dropout activated $\{\widehat{\mathbb{y}}^{(m)}(\mathbb{x})\}_{m=1}^{M}$.

Here, each stochastic prediction $\widehat{\mathbb{y}}^{(m)}(\mathbb{x})$consists of both the predicted mean $\mu^{(m)}$and the predicted variance $\sigma^{(m)}$, representing the network output for heteroscedastic uncertainty estimation. In this study, only the $\mu$and varestimates within the 95% confidence interval are retained as credible uncertainty prediction results for subsequent analysis.

3. Proposed methodologies

3.1. Task-driven adaptive VMD approach for degradation indicator construction

The quality and reliability of VMD largely depend on two key parameters: the penalty factor α and the number of decomposition modes K. A well-chosen combination of α and K is critical for extracting degradation information from the raw dynamics. To address this issue, an adaptive VMD approach is proposed in this section for effective degradation feature extraction by formulating the parameters selection as an optimization problem [46].

The TDA-VMD is designed to decompose the target dynamics into Intrinsic Mode Functions (IMFs) that carry precise and reliable information. To achieve this, the first step, in Eq. (20), is to evaluate each individual IMF by measuring its information entropy, ensuring that the extracted components retain the most informative and meaningful content. The second objective is to minimize the correlation between IMFs, in Eq. (21), which helps avoid mode mixing and ensures a clearer separation of dynamic features. This is addressed by calculating the mutual information between IMFs.

$$f_1 = \frac{1}{\mathrm{K}}\sum_{i=1}^{\mathrm{K}} Entropy(\mathrm{IMF}_i) \tag{20}$$

$$f_2 = \frac{2}{\mathrm{K}(\mathrm{K}-1)}\sum_{i=1}^{\mathrm{K}}\sum_{j=i+1}^{\mathrm{K}} MI(\mathrm{IMF}_i, \mathrm{IMF}_j) \tag{21}$$

.

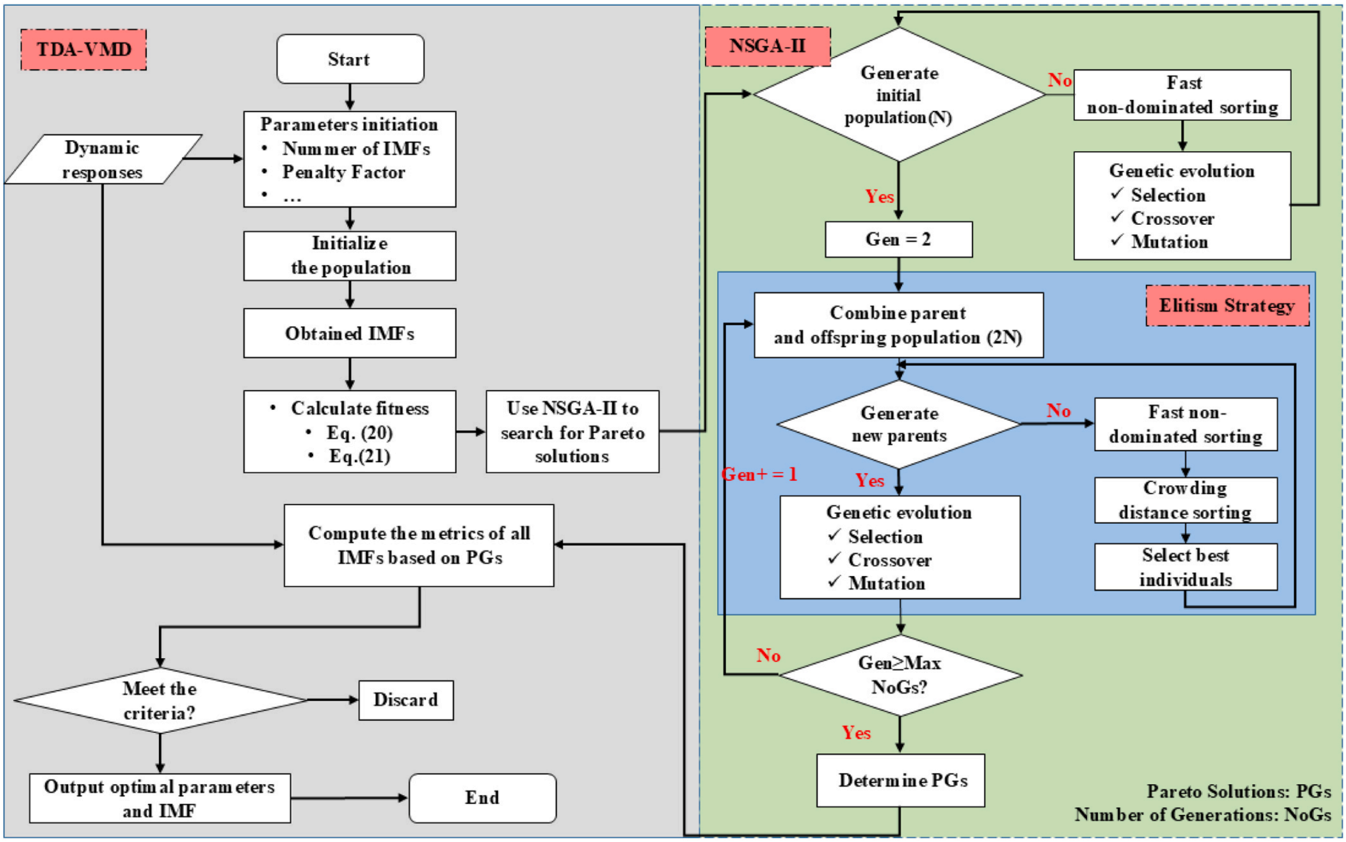

Fig. 2. TDA-VMD optimization workflow.

Table 2
Sensitivity analysis of NSGA-II hyperparameters (average computational time, s).

Population Size	Generation= 20	Generation= 30	Generation= 50
30	9.85–11.68	14.23–15.56	24.45–25.76
50	15.02–16.08	22.62–23.73	36.54–39.01
70	21.86–23.98	33.18–35.64	33.18–35.64

Table 3
Time-domain statistical parameters and frequency-domain features.

Features	Definition	Features	Definition
Standard Deviation	$\sigma = \sqrt{\sum_{i=1}^{n}(x-\bar{x})^2(n)^{-1}}$	Crest Factor	$CF = \max(x)/RMS$
Skewness	$S_k = \mu_3/\sigma_3$	Shape Factor	$SF = RMS/(\sum_{i=1}^{n}\lvert x_i\rvert/n)$
Kurtosis	$K = \mu_4 - \sigma^4$	Impulse Factor	$IF = \max(x)/(\sum_{i=1}^{n}\lvert x_i\rvert/n)$
Peak-to-Peak Value	$x_{Peak2Peak} = \max(x) - \min(x)$	Margin Factor	$MF = \max(x)/(\sum_{i=1}^{n}\lvert x_i\rvert/n)^2$
Root Mean Square	$RMS = \sqrt{\sum_{i=1}^{m}x_i^2(n)^{-1}}$	Energy	$E = \sum_{i=1}^{n}x_i^2$

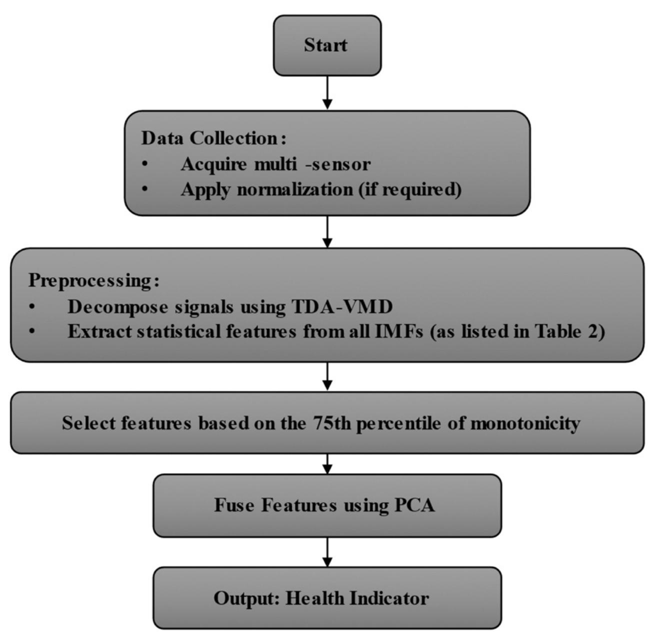

Fig. 3. TDA-VMD-based HI construction process.

Fig. 3 presents the flowchart of the proposed Task-Driven Adaptive VMD approach (TDA-VMD) based on NSGA-II.

As shown in Fig. 2, the proposed TDA-VMD method uses the dynamic response signal of the FOWT platform as input. The signal is first decomposed into several IMFs by VMD. Information entropy and mutual information are then used as two optimization objectives to retain informative dynamic features and reduce redundancy between IMFs. Based on these objectives, NSGA-II is applied to optimize the VMD parameters through selection, crossover, and mutation. After convergence, the selected parameter set is used to obtain the final IMFs. To determine the NSGA-II settings, a grid search was conducted over mutation rate, crossover rate, number of generations, and population size, as shown in Table 2. In total, 36 configurations were tested, with an average computational cost ranging from 9.2 s to 55.3 s per run.

In the context of structural health monitoring for FOWT

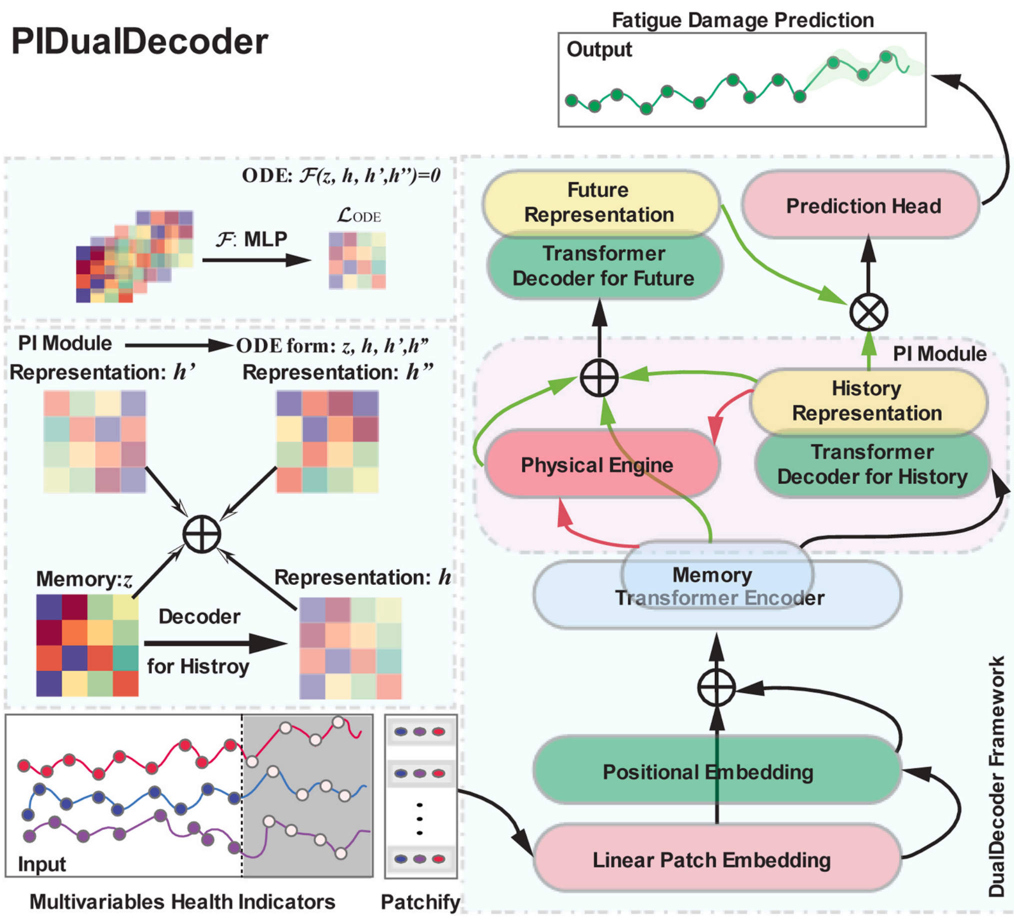

Fig. 4. PIDualDecoder framework.

substructures, time-domain statistical measures and frequency-domain features are commonly used to characterize the health state of the system. Prior to feature extraction, the acquired signals are first processed using the proposed TDA-VMD method to perform filtering and mode decomposition. Table 3 lists the typical time-domain and frequency-domain features extracted from responses.

The third-order central moment is used for computing skewness, while the fourth-order central moment is used for calculating kurtosis. The reliability and efficiency of TDA-VMD in degradation quantification will be validated in Section 5.

Based on the features listed in Table 3, 10 candidate features are extracted at each time step. The TDA-VMD procedure, as shown in Fig. 3, is used to construct a feature pool, from which the final health indicator (HI) is obtained using PCA. A percentile-based threshold is applied for feature selection, and the 75th percentile is used in this study. This threshold balances retaining informative features and reducing noise-dominated features before PCA-based fusion [47–49]. It is used as a heuristic setting and can be adjusted for different applications.

3.2. Physics-informed dual decoders learning framework

Although $p_\theta(\mathbf{Y}_{1:S}|\mathbf{X}_{1:k})$ offers a unified formulation for degradation modeling, it does not distinguish historical reconstruction from future forecasting. The former mainly refines observed information, whereas the latter extrapolates latent dynamics beyond the observed horizon. Using a shared decoder may therefore weaken forecasting-specific inductive bias. To address this, we propose a DualDecoder framework that separates history and future decoding [50,51]. The history decoder organizes latent representations of observed sequences, while the future decoder generates future-oriented representations conditioned on the historical representation. This design introduces a more suitable inductive bias for prognostics, as future degradation should be inferred from the underlying historical state evolution instead of the historical measurements themselves. However, separating historical and future decoding alone is still insufficient for reliable long-horizon prediction. The future state is not only determined by historical representations, but also by the dynamic transition law governing the evolution from history to future. Motivated by the general form of ordinary differential equations [52], further introducing a PIDualDecoder, in which a physics-inspired module is incorporated to model the dynamic coupling between historical and future representations. In this way, the proposed framework enhances the structural inductive bias of the model and improves its ability predict the fatigue life.

Fig. 4 illustrates the statistical learning formulation underlying the proposed PIDualDecoder. Unlike the conventional one-stage objective $p_\theta(\mathbb{Y}_{1:S}|\mathbb{X}_{1:k})$, the proposed framework reformulates prognostic learning as a hierarchical conditional prediction problem. Specifically, the historical segment is first reconstructed from the observed input sequence through $p_{\theta_h}(\mathbb{Y}_{1:S}|\mathbb{X}_{1:k})$, which yields both the historical prediction $\widehat{\mathbb{Y}}_{1:k}$and its latent representation $\mathbb{H}_{1:k}$. The future segment is then predicted conditionally on these intermediate historical outputs, rather than directly on the raw observations, i.e.,$p_{\theta_f}(\mathbb{Y}_{k+1:S}|\widehat{\mathbb{Y}}_{1:k}, \mathbb{H}_{1:k})$. Accordingly, the overall conditional distribution is factorized as:

$$p_\theta(\mathbb{Y}_{1:S}|\mathbb{X}_{1:k}) = p_{\theta_h}(\mathbb{Y}_{1:S}|\mathbb{X}_{1:k})\, p_{\theta_f}(\mathbb{Y}_{k+1:S}|\widehat{\mathbb{Y}}_{1:k}, \mathbb{H}_{1:k}) \tag{22}$$

which explicitly encodes the inductive bias that future degradation should be inferred from the reconstructed historical state and its latent representation. Based on this factorization, the DualDecoder objective is

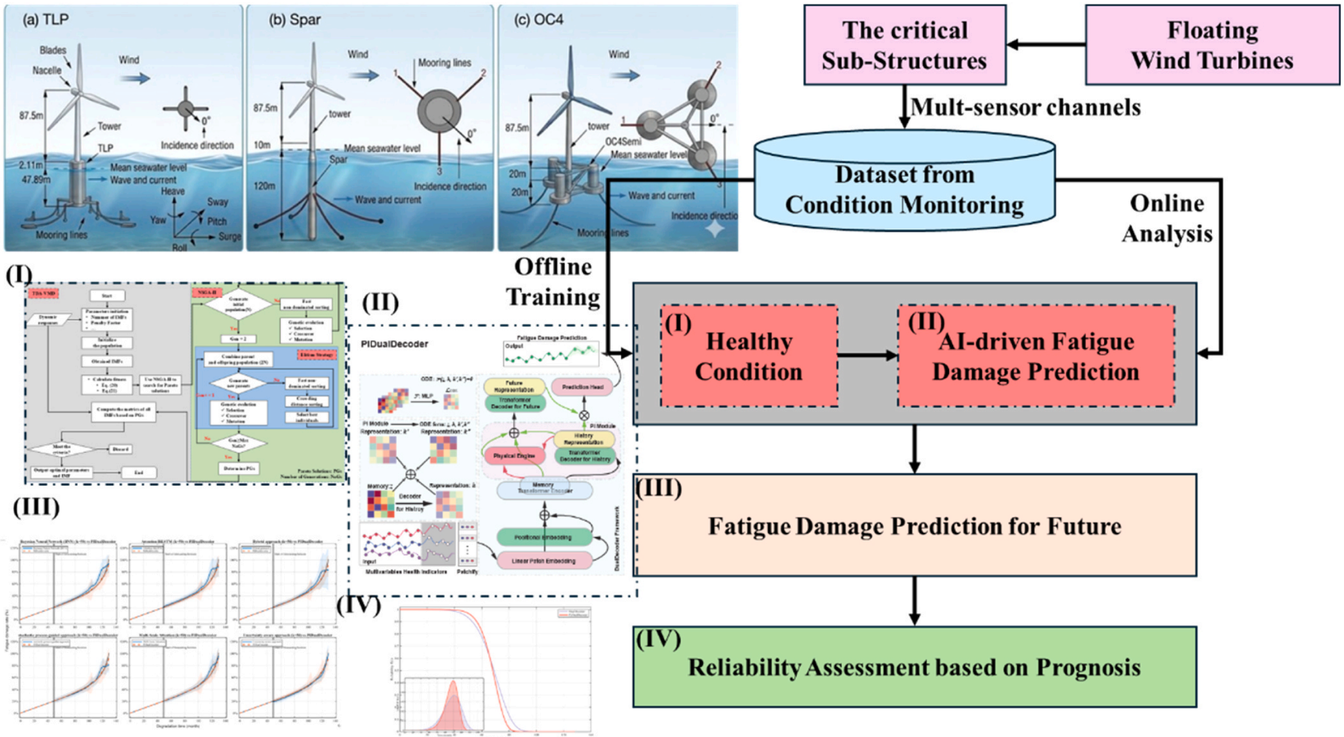

Fig. 5. Prognosis framework for FOWT substructures.

defined as:

$$\mathscr{L}_{\text{Data}} = -\mathscr{L}_{\text{hist}}\log p_{\theta_h}(\mathbb{Y}_{1:S}|\mathbb{X}_{1:k}) - \mathscr{L}_{\text{fut}}\log p_{\theta_f}(\mathbb{Y}_{k+1:S}|\widehat{\mathbb{Y}}_{1:k},\mathbb{H}_{1:k}) \tag{23}$$

.

Furthermore, to capture the dynamic coupling between historical and future representations, a physics-informed regularization is introduced through an ODE-motivated latent evolution constraint, $\mathscr{F}_\phi(\mathbf{z}_t, \hbar_t, \dot{\hbar}_t, \ddot{\hbar}_t) = 0$. For Learning, Given the observed input sequence $\mathbb{X}_{1:k}$, the encoder first maps it into a memory representation $\mathbb{Z}_{1:k}$. A history decoder then produces both the reconstructed historical outputs $\widehat{\mathbb{Y}}_{1:k}$and the corresponding latent history representation $\mathbb{H}_{1:k}$. Based on $(\mathbb{Z}_{1:k}|\mathbb{H}_{1:k})$, the PI module further extracts latent evolution quantities $\mathbb{H}'_{1:k} = \frac{d\mathbb{H}_{1:k}}{d\mathbb{Z}_{1:k}}$and $\mathbb{H}''_{1:k} = \frac{d^2\mathbb{H}_{1:k}}{d\mathbb{Z}_{1:k}^2}$ into a physics-informed relation code $\mathbb{C}_{1:k}$. The future decoder subsequently predicts the future representation conditioned on $\mathbb{Z}_{1:k}$, $\mathbb{H}_{1:k}$, and $\mathbb{C}_{1:k}$, rather than directly on the raw historical observations. Therefore, the future predictive distribution is formulated as $p_{\theta_f}(\mathbf{Y}_{k+1:S}|\mathbb{Z}_{1:k}, \mathbb{H}_{1:k}, \mathbb{C}_{1:k})$. Moreover, the physics-informed regularization is defined by penalizing the residual of an ODE-inspired latent evolution law: $\mathscr{L}_{\text{PI}} = \left\|\mathscr{F}_\phi(\mathbf{z}_t, \hbar_t, \dot{\hbar}_t, \ddot{\hbar}_t)\right\|_1$, leading to the final PIDualDecoder objective: $\mathscr{L}_{\text{total}} = \mathscr{L}_{\text{Data}} + \mathscr{L}_{\text{PI}}$. To avoid manual tuning of the task weights, the balance among $\mathscr{L}_{\text{hist}}$, $\mathscr{L}_{\text{fut}}$, and $\mathscr{L}_{\text{PI}}$is adaptively adjusted using the uncertainty-based weighting strategy [53].

3.3. *Uncertainty-aware conditional reliability assessment based on prognosis*

Reliability is evaluated based on stochastic damage accumulation driven by the prognostic results. For each sample, the prognostic model provides the predictive mean $\mu(t)$ and standard deviation $\sigma(t)$ over the future horizon. Let $D(t)$denote the cumulative damage state at time t, and let δ be the failure threshold. The failure time is defined as:

$$T = \inf\{t \geq 0 : D(t) \geq \delta\} \tag{24}$$

.

Because the system is already known to be safe up to the current observation instant t_k, only the future evolution after $t_k$is treated as uncertain. Therefore, the conditional reliability is defined as:

$$\mathbb{R}(t|t_k) = \mathbb{P}(T > t|T > t_k), t > t_k \tag{25}$$

.

At each future time step t_j, the damage growth rate is sampled according to the predictive distribution:

$$r(t_j) \sim \mathscr{N}(\mu(t_j), \sigma^2(t_j)) \tag{26}$$

where $r(t_j)$is constrained to be non-negative to preserve physical interpretability. The cumulative damage is then updated recursively as:

$$D(t_j) = D(t_{j-1}) + r(t_j)\Delta t_j \tag{27}$$

where $\Delta t_j = t_j - t_{j-1}$. For the m-th Monte Carlo trial, the failure time is determined as the first passage time when the cumulative damage reaches the failure threshold:

$$T^{(m)} = \inf\{t_j \geq t_k : D^{(m)}(t_j) \geq \delta\}, m = 1, 2, \ldots, N_{\text{MC}} \tag{28}$$

.

After repeating this simulation process over N_{MC} trials, a set of stochastic failure times is obtained. To describe the lifetime distribution in a compact parametric form, these failure times are fitted using a two-parameter Weibull distribution with probability density function:

$$f_T(t) = \frac{\beta}{\eta}\left(\frac{t}{\eta}\right)^{\beta-1}\exp\left[| \left(\frac{t}{\eta}\right)^{\beta}\right] \tag{29}$$

.

The corresponding reliability function is then written as:

$$\mathbb{R}(t) = \exp\left[| \left(\frac{t}{\eta}\right)^{\beta}\right] \tag{30}$$

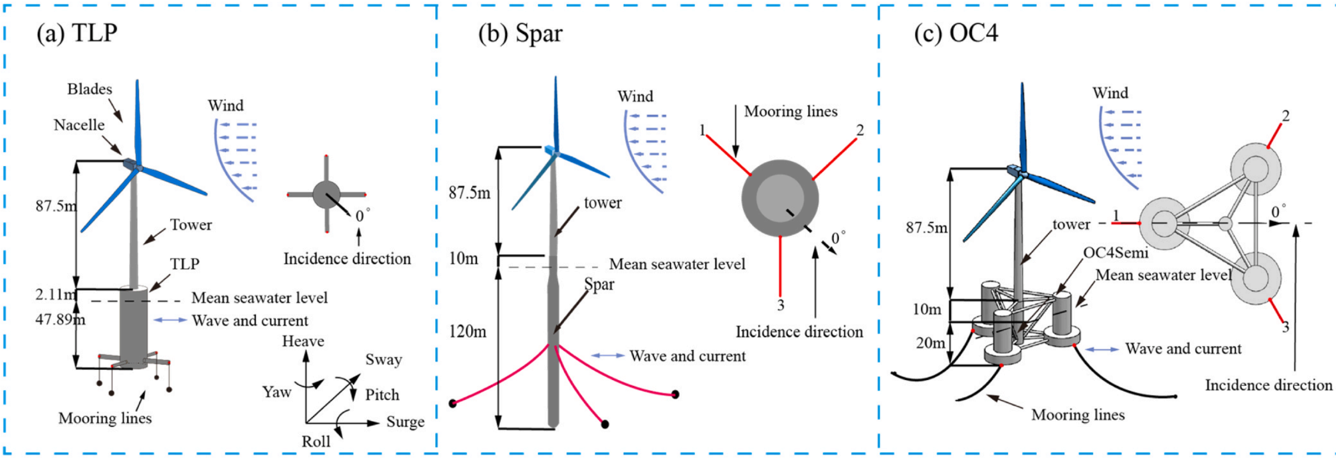

(a) TLP (b) OC3-Hywind Spar (c) OC4-DeepCwind -

Fig. 6. FOWT configurations used for validation.

Table 4
The detailed properties of three platforms.

Platforms	Depth of draught (m)	Total mass (kg)	Displaced volume (m^3)	Total mooring top Tension (N)
TLP	50	8.6×10^6	12179.6	3.2×10^7
OC3Spar	120	7.47×10^6	8029	2.7×10^6
OC4Semi	30	3.85×10^6	13917	3×10^6

Table 5
The details of examined simulation scenario.

Wind Speed (m/s)	Significant Wave Height (m)	Peak Frequency (Hz)	Current Speed (m/s)
4	1.95	9.73	0.08
8	2.48	9.83	0.16
11	2.96	10.01	0.22
15	3.66	10.31	0.31
18	4.23	10.57	0.36

Table 6
Hyper parameters setting.

Component	Setting / Value
Mini-batch size	64
Initial learning rate	5×10^{-4}
Optimizer	AdamW
Learning rate decay	50 epochs with 0.9 decay
Uncertainty modeling	Prior variance = 0.1
Backbone architecture	Transformer
Early Stopping Criteria	Validation loss does not improve
Transformer heads	16
Embedding dimension	128
Latent space size	128
Number of sensors	6

.

Conditioned on survival up to the current time t_k, the conditional reliability is finally obtained as:

$$\mathbb{R}(t|t_k) = \frac{\mathbb{R}(t)}{\mathbb{R}(t_k)}, t > t_k \tag{31}$$

.

In this way, the proposed framework transforms the predictive mean and uncertainty of the degradation model into a probabilistic reliability description, thereby providing a dynamic and uncertainty-aware basis for maintenance planning and risk-informed decision-making.

3.4. *Intelligent prognostic framework for FOWT sub-structures*

Based on the proposed health indicator construction method and the PIDualDecoder, a comprehensive FOWT prognosis framework is developed as shown in Fig. 5.

Fig. 5 shows the proposed prognosis framework for critical sub-structures of FOWTs. The six-DOF acceleration responses are first processed in Step (I) to construct six health indicators (HIs). In Step (II), these HIs are used as the input of the PIDualDecoder model. The model output is the fatigue damage corresponding to the six HIs. Step (III) predicts the future evolution of fatigue damage, and Step (IV) uses the predicted damage for reliability assessment.

4. Simulation-based dataset generation and prognostic framework setup

4.1. *FOWT simulation environment*

To validate the proposed damage quantification and prognosis framework, three representative floating offshore wind turbine (FOWT) configurations, as shown in Fig. 6, were established in OpenFAST, namely the OC3-Hywind Spar, OC4-DeepCwind Semi-submersible, and Tension Leg Platform (TLP).

A virtual structural health monitoring system is established within the OpenFAST simulation environment. The monitoring system records the six-degree-of-freedom (6-DOF) platform accelerations, including surge, sway, heave, roll, pitch, and yaw accelerations. These dynamic response signals serve as the input measurements of the proposed prognosis framework. The signals are sampled at 80 Hz throughout the entire degradation process. The main characteristics of the three floating platforms are summarized in Table 4, including the draft depth, total structural mass, displaced volume, and total mooring pretension. For a more comprehensive assessment, the TLP model considers multidirectional irregular wave loading, whereas the OC3Spar and OC4Semi models are simulated under unidirectional irregular wave conditions.

To account for different environmental conditions encountered during offshore operation, fatigue degradation simulations are conducted under multiple environmental and operating conditions (EOCs), as listed in Table 5.

The stochastic environmental loads are generated using wind-wave coupled spectral models characterized by wind speed, significant wave

Table 7
Design of prognosis validation scenarios.

Scenario ID	Training Wind Speed (m/s)	Testing Wind Speed (m/s)	Prediction Mode
T1-TLP	4–18	4–18	Start at 25 months
T2-OC4Semi	4–18	4–18	Start at 50 months

height, peak wave frequency, and current velocity.

4.2. *Prognostic scenario and hyperparameter setup*

In this study, the key hyperparameters, as shown in Table 6, were selected according to the actual training configuration to ensure stable optimization and robust prognostic performance. To better reflect realistic prognostic conditions, a no-cheating setting was adopted, where the model predicted future degradation only from observed historical sequences. A length mask was used to handle sequences with different valid lengths. For fair comparison, all models were trained using the same data partition, optimizer, learning rate, batch size, epochs, and forecasting protocol. Cross-wind-speed prediction scenarios were designed to evaluate the generalization ability of the proposed method, as summarized in Table 6.

To validate the proposed prognosis framework, three validation scenarios were designed for different FOWT platform types, as listed in Table 7. From a sequence-learning perspective, the model input is a multi-dimensional historical time series constructed from the six health indicators derived from the 6-DOF acceleration responses. The model output is a one-dimensional future fatigue sequence, representing the predicted fatigue damage evolution of the monitored mooring system.

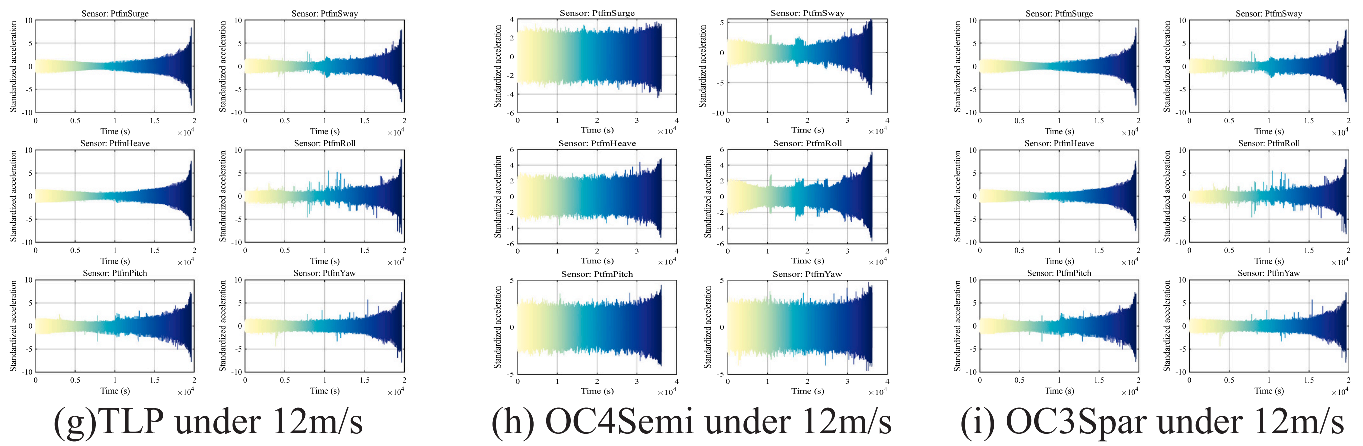

Fig. 7. Comparative time-domain dynamics of FOWT platforms under fatigue-induced degradation.

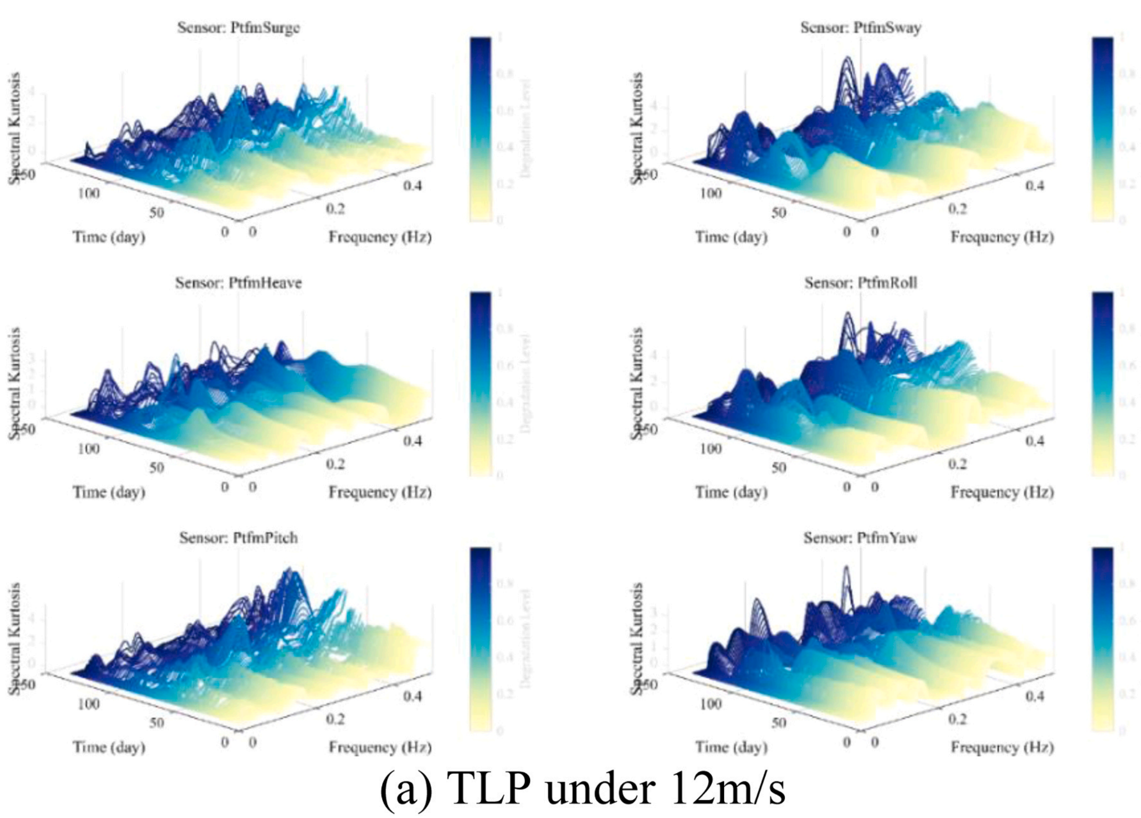

Fig. 8. Directional sensitivity of spectral kurtosis to fatigue damage in FOWT substructures.

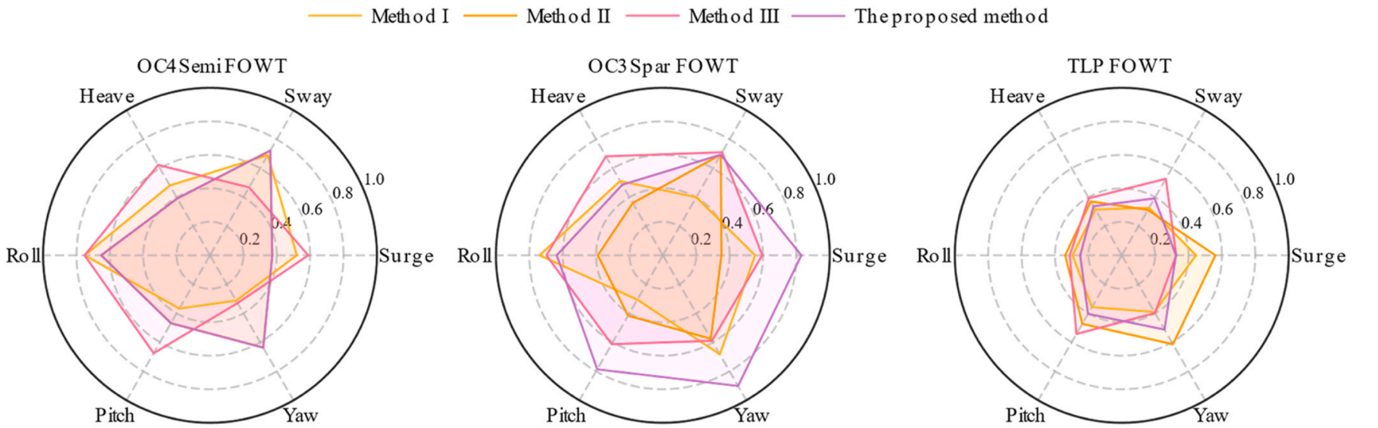

Fig. 9. Comparative evaluation of HI performance across multiple sensors.

Table 8
Sensor suitability for health indicator.

Sensor	Average Score: (TLP+OC3 +OC4)/3
Sway	0.555
Yaw	0.548
Roll	0.539
Pitch	0.492
Surge	0.487
Heave	0.446

Table 9
Overall performance of. the HI construction methods. on selected sensors.

	Average Score
The proposed method	**0.600**
(Method I)	0.510
(Method II)	0.548
(Method III)	0.532

Therefore, the task is formulated as a sequence-to-sequence prognosis problem, where historical multi-dimensional degradation information is used to predict future fatigue progression.

4.3. Evaluation metrics

To evaluate the constructed HI, three metrics are used: monotonicity, prognosability, and trendability. For each HI construction method, the average of the three metrics is calculated to compare the overall HI quality across different methods and structural configurations:

$$Score_{i,j} = \frac{\text{monotonicity}_{i,j} + \text{prognosability}_{i,j} + \text{trendability}_{i,j}}{3} \tag{32}$$

.

where i denote the structure (e.g., OC3, OC4, or TLP), and j represents the HI construction method.

The root mean square (RMSE) and mean absolute (MAE) of the prediction error and mean relative accuracy (MRA) are used to evaluate the performance of the predicted fatigue. RMSE, MAE, and MRA are respectively defined as [54]:

$$\text{RMSE} = \sqrt{\frac{1}{K}\sum_{k=1}^{K}\left(PredDamage_k - RealDamage_k\right)^2} \tag{33}$$

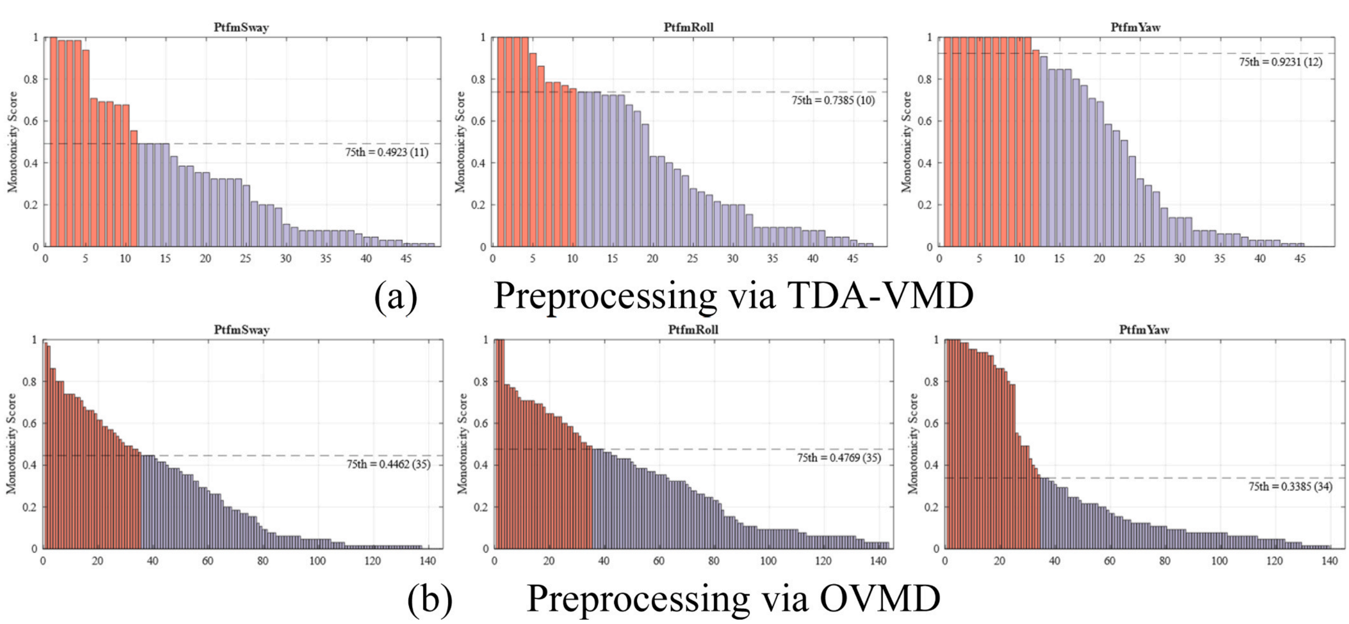

Fig. 10. Performance comparison of OVMD and TDA-VMD methods on different sensors.

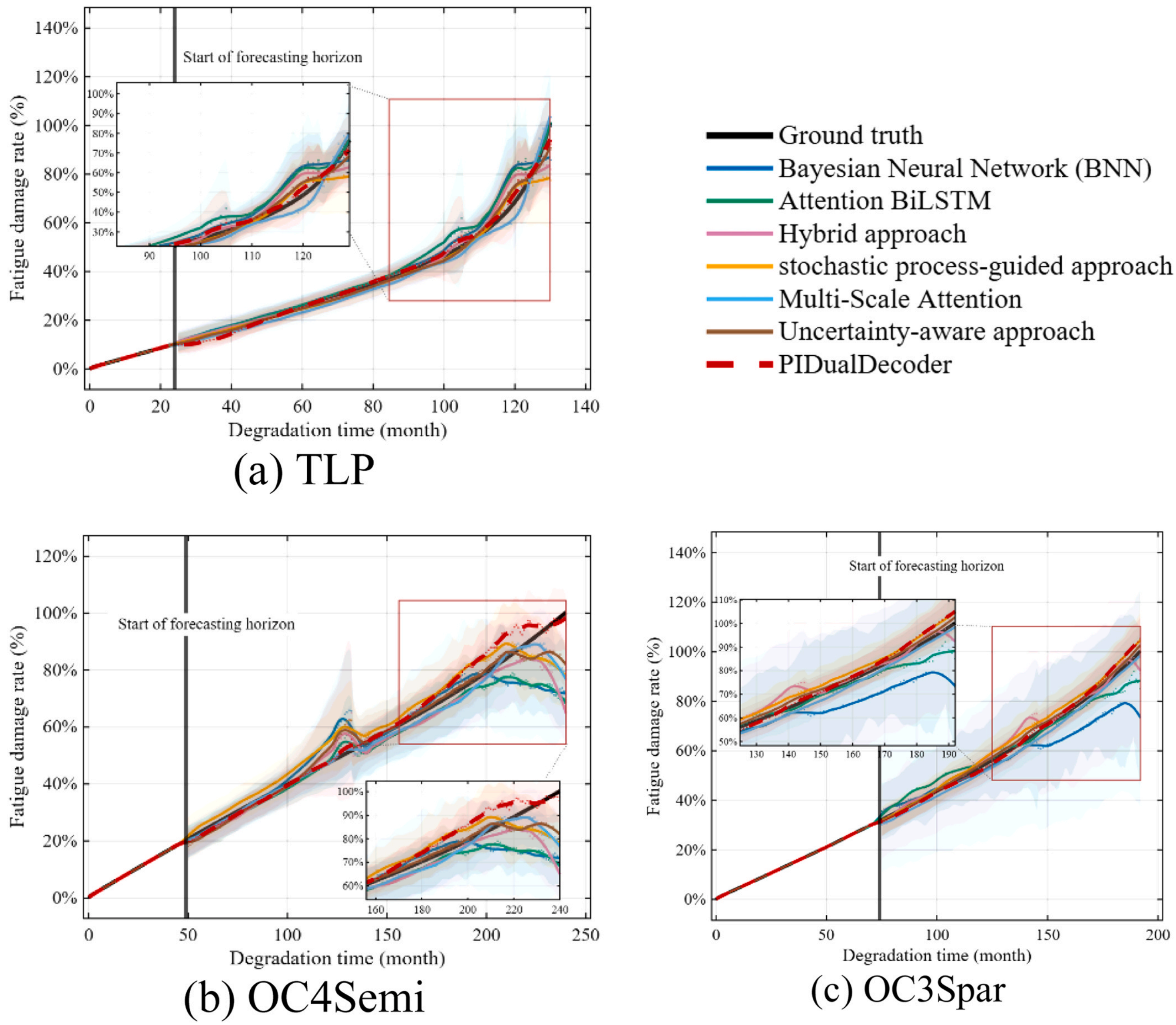

Fig. 11. Prognostic result for three types in early degradation stage.

$$\mathrm{MAE} = \frac{1}{K}\sum_{k=1}^{K} |(PredDamage_k - RealDamage_k| \tag{34}$$

$$\mathrm{MRA} = \sum_{k=1}^{K} RA_k, RA_k = 1 - \frac{|PredDamage_k - RealDamage_k|}{RealDamage_k} \tag{35}$$

where *PredDamage* is the predicted fatigue damage, *RealDamage* is real damage. SF punishes positive error more than negative error compared with RMSE and MRA ranges from $-\infty$ to 1, with preferred prediction obtained when MRA is close to 1.

5. Discussion and analysis

5.1. Dynamic analysis for substructures of FOWT under degradation

Degradation of FOWT substructures can change the system dynamic responses under wind, wave, and current loads. Fig. 7 shows the response variations caused by mooring system degradation for three FOWT platforms: TLP, OC4Semi, and OC3Spar.

Fig. 7 shows the time-domain acceleration responses of the TLP, OC4Semi, and OC3Spar platforms under mooring fatigue degradation at 12 m/s. Clear differences can be observed among the three platform types. The TLP exhibits the most stable response due to its high restoring stiffness, while the OC4Semi shows moderate sensitivity to mooring degradation. The OC3Spar is the most sensitive platform, particularly in pitch and yaw, owing to its low-frequency motion characteristics and larger hydrodynamic inertia. These results suggest that the effect of mooring fatigue degradation is strongly platform-dependent. The corresponding frequency-domain responses at 12 m/s are analysed next.

Fig. 8 provides spectral kurtosis analysis under a 12 m/s wind speed confirms the effectiveness of the proposed fatigue degradation simulation framework for the TLP platform. As fatigue accumulates, non-stationary features become more evident, especially in Pitch and Roll. Pitch shows a clear frequency shift from about 0.15 Hz to 0.25 Hz, while Roll presents enhanced transient responses. These results indicate that spectral kurtosis can capture fatigue-induced dynamic changes and support damage assessment, condition monitoring, and predictive maintenance of floating offshore wind turbines.

Table 10
Quantitative evaluation of damage prediction results.

Method	Types of FOWT	RMSE	MAE	MRA
Bayesian Neural Network	OC4Semi	7.81 ± 1.23	5.17 ± 1.69	0.92 ± 0.017
	TLP	4.85 ± 2.62	2.41 ± 1.34	0.95 ± 0.025
	OC3Spar	11.12 ± 7.96	10.44 ± 7.53	0.76 ± 0.172
Attention BiLSTM	OC4Semi	7.61 ± 3.12	5.12 ± 2.24	0.91 ± 0.043
	TLP	4.48 ± 2.59	2.67 ± 1.31	0.94 ± 0.023
	OC3Spar	6.21 ± 8.77	5.47 ± 7.61	0.88 ± 0.153
Hybrid approach	OC4Semi	7.28 ± 2.61	5.17 ± 1.71	0.91 ± 0.037
	TLP	4.35 ± 2.54	2.22 ± 1.28	0.96 ± 0.021
	OC3Spar	5.62 ± 10.76	4.61 ± 9.46	0.92 ± 0.222
stochastic process-guided approach	OC4Semi	7.14 ± 1.73	4.31 ± 1.05	0.92 ± 0.0217
	TLP	3.94 ± 1.87	2.10 ± 0.79	0.95 ± 0.024
	OC3Spar	5.61 ± 10.18	4.67 ± 9.40	0.91 ± 0.223
Multi-Scale Attention	OC4Semi	6.39 ± 2.81	3.90 ± 1.79	0.93 ± 0.032
	TLP	3.87 ± 2.45	1.90 ± 0.96	0.96 ± 0.016
	OC3Spar	5.54 ± 3.87	5.10 ± 3.67	0.85 ± 0.073
Uncertainty-aware approach	OC4Semi	5.61 ± 1.68	3.80 ± 1.10	0.92 ± 0.021
	TLP	3.83 ± 2.17	2.64 ± 1.31	0.93 ± 0.021
	OC3Spar	3.61 ± 3.39	3.12 ± 3.08	0.93 ± 0.061
PIDualDecoder	OC4Semi	5.17 ± 3.11	3.72 ± 2.16	0.92 ± 0.039
	TLP	3.12 ± 1.71	1.81 ± 0.81	0.98 ± 0.014
	OC3Spar	2.85 ± 2.33	2.53 ± 2.24	0.93 ± 0.049

5.2. Validation of TDA-VMD for degradation quantification

The quality and uncertainty of the proposed degradation indicators are evaluated using the hybrid metric under fluctuating wind and unsteady wave conditions, with comparison against three state-of-the-art methods: spectral kurtosis with principal component analysis (Method I) [55], spectral kurtosis with principal component analysis with optimized VMD (Method II) [56], and an autoencoder-based degradation indicator (Method III) [57]. Fig. 9 compares four degradation quantification methods, including three baseline methods (Method I–III) and the proposed method, across six sensor types for the OC4Semi, OC3Spar, and TLP platforms.

Clear differences can be observed among methods, sensors, and platform types. Overall, the proposed method shows the best or competitive performance for most sensor categories, especially on the OC4Semi and OC3Spar platforms, while the TLP responses are generally less sensitive. The average prognostic metric score of each sensor is further summarized in Table 8. Accordingly, Sway, Yaw, and Roll are selected as the main sensor channels for HI construction and prognostics.

Table 9 shows that the proposed method achieves the best overall performance on these sensors, with an average score of 0.600, compared with 0.510, 0.548, and 0.532 for Methods I–III, respectively.

This improvement is attributed to the TDA-VMD-based feature construction, which provides a richer set of effective features for subsequent PCA-based HI fusion. A comparison of the number of effective features obtained by the proposed method and the optimized single-objective VMD method is presented in Fig. 10.

Fig. 10 compares the monotonicity scores of candidate features extracted from the Sway, Roll, and Yaw channels using TDA-VMD and OVMD. The results show that TDA-VMD produces features with stronger monotonic degradation trends and higher 75th-percentile scores across all three sensors. In contrast, although OVMD generates more candidate features, their overall monotonicity is lower. This indicates that TDA-VMD is more effective in extracting degradation-sensitive features for subsequent HI construction.

5.3. Validation of the prognostics with SOTA approaches

To validate the reliability and generalizability of the proposed method in predicting sub-structures of floating wind turbines, this section compares the proposed approach with several state-of-the-art (SOTA) models including Bayesian Neural Network [40], Attention BiLSTM [16], Hybrid approach [23], stochastic process-guided approach [58], Multi-Scale Attention [59] and Uncertainty-aware approach [60]. Fig. 11 and Table 10 give comparison focuses on prediction results for different months prior to failure.

As shown in Fig. 11, all methods can fit the historical degradation data reasonably well before the forecasting horizon. However, clear

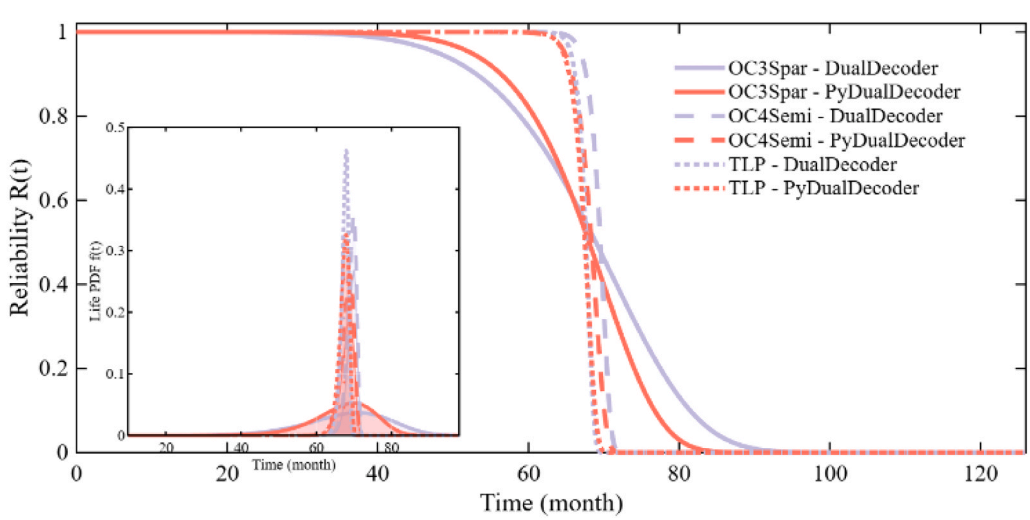

Fig. 12. reliability assessment under prognosis results.

differences appear during prediction. Compared with the benchmark methods, PIDualDecoder follows the true damage trajectory more closely and provides more stable forecasts across the three FOWT platforms. For the TLP-FOWT case, PIDualDecoder maintains good agreement with the reference degradation curve, especially in the later prediction stage. For the OC4Semi-FOWT case, where the degradation behaviour is more complex, the proposed method still captures the increasing damage trend more effectively than the baselines. For the OC3Spar-FOWT case, PIDualDecoder also shows better consistency, while several competing methods exhibit larger deviations or fluctuations. Overall, the results in Fig. 11 and Table 10 demonstrate that PIDualDecoder provides more accurate and robust early-stage fatigue damage prediction. Its ability to capture both global degradation trends and local damage variations makes it suitable for early warning, health assessment, and predictive maintenance of floating offshore wind turbines.

5.4. Uncertainty analysis on prognostic performance and reliability assessment

This section evaluates the uncertainty of the predicted fatigue lifetime and its influence on reliability assessment for the three FOWT platforms.

As shown in Fig. 12, the physics-informed PIDualDecoder produces a more concentrated failure distribution than the purely data-driven DualDecoder across the three FOWT platforms. This is reflected by the sharper lifetime probability density and the steeper reliability transition, indicating a more clearly defined high-risk period. This improvement is important for maintenance decision-making. A broad failure distribution leads to greater uncertainty in identifying the critical degradation stage, which may result in either delayed intervention or overly conservative maintenance. In contrast, the narrower distribution obtained by PIDualDecoder reduces uncertainty in failure timing and provides a more actionable maintenance window. Therefore, the main value of the physics-informed framework is not simply predicting an earlier or later lifetime, but providing a clearer reliability characterization. This supports more confident inspection planning, preventive maintenance scheduling, spare-part preparation, and offshore operation management.

6. Conclusion

Reliable O&M strategies are essential for reducing the lifecycle cost of FOWTs. This study proposed a prognosis framework for the health assessment of FOWT substructures, integrating TDA-VMD-based HI construction, a Physics-Informed Dual Decoder model for fatigue damage prediction, and a prognosis-based reliability assessment module. The framework was validated on three types of FOWTs, demonstrating its effectiveness in health monitoring, fatigue prognosis, and reliability evaluation. The main conclusions are as follows:

1) Fatigue degradation of substructures, particularly in mooring lines, may alter the dynamic response frequencies of the platform. As degradation progresses, these responses may approach structural modal frequencies, increasing the risk of adverse dynamic behaviour. This highlights the importance of timely health assessment for FOWT substructures.
2) Based on platform dynamic responses, the constructed HI showed that Sway, Roll, and Yaw are the most informative sensor channels among the six platform degrees of freedom for representing structural degradation. This result highlights the value of multi-sensor dynamic information for fatigue damage prediction and RUL assessment.
3) The proposed PIDualDecoder model achieved superior performance in fatigue damage prediction compared with benchmark methods. By introducing physics-informed inductive bias into the latent fatigue evolution, the model provides more physically consistent and reliable prognosis, thereby supporting more credible reliability assessment and reducing unnecessary O&M interventions.

Limitations and future work

A limitation of the present study is that the proposed framework still depends on relatively large training datasets, which may limit its applicability when fatigue monitoring data are sparse or incomplete. Future work will therefore focus on reducing data dependence and developing more knowledge-driven approaches for fatigue prognosis in complex environments. In particular, the integration of symbolic AI with prognostic modelling will be investigated to better incorporate physical knowledge, causal relationships, and rule-based reasoning, thereby improving model generalizability and reliability under limited-data conditions.

Declaration of Competing Interest

The authors declare that they have no known competing financial interests or personal relationships that could have appeared to influence the work reported in this paper.

Acknowledgment

This study was funded by the Natural Science Foundation of Shanghai Municipality (No. 24ZR1454800), the State Key Laboratory of Mechanical System and Vibration (Grant No. MSV202411), and the National Natural Science Foundation of China (Grant No. 52506259). The author gratefully acknowledges the University of Liverpool for hosting his Marie Curie Fellowship (EPSRC EP/Y014235/2).

Data Availability

No data was used for the research described in the article.

References

[1] Hu W, E J, Leng E, Zhang F, Chen J, Ma Y. Energy 2023;263.
[2] Hu W, E J, Tan Y, Zhang F, Liao G. Energy 2022;247.
[3] Wei K, Yang Y, Zuo H, Zhong D. Wind Energy 2020;23:433–57.
[4] Xu Z, Zhao K, Zhang W, Miao W, Sun K, Wang J, et al. J Ind Inf Integr 2025;46.
[5] Zhu Y, Guo T, Li X, Zhang Y, Zhang W. J Dyn Monit Diagn 2024;3:311–23.
[6] Hadjoudj Y, Pandit R. Energy Sci Eng 2022.
[7] Jiang G, Li D, Feng K, Li Y, Zheng J, Ni Q, et al. J Dyn Monit Diagn 2023;2:275–89.
[8] Sun S, Wang T, Chu F. Renew Sustain Energy Rev 2022;160:112326.
[9] Xu Z, Bashir M, Zhang W, Yang Y, Wang X, Li C. Inf Fusion 8687 2022:17–29.
[10] Cai Q, Wang J, Dai K, Cheng Y, Li Y, Ma W, et al. Ocean Eng 2025;318.
[11] Xu Z, Li C, Yang Y. ISA Trans 2021;110:379–93.
[12] Xu Z, Bashir M, Yang Y, Wang X, Wang J, Ekere N, et al. Renew Energy 2022;199: 21–34.
[13] Wang Y, Peng Y, Zi Y, Jin X, Tsui KL. IEEE Trans Ind Inform 2016;12:924–32.
[14] Li H, Ding Y, Sun Y, Xie M, Guedes Soares C. Reliab Eng Syst Saf 2025;261.
[15] Liu X, Song P, Yang C, Hao C, Peng W. IEEE Trans Ind Electron 2017;65:1549–58.
[16] Xu Z, Bashir M, Liu Q, Miao Z, Wang X, Wang J, et al. Comput Ind Eng 2023;176: 108999.
[17] M. Bashir, Z. Xu, J. Wang, (2022).
[18] Qiu G, Ye B, Gu Y, Huang P, Li H, Xu Z. IEEE Sens J 2025.
[19] Lu Y, Sun L, Zhang X, Feng F, Kang J, Fu G. Appl Ocean Res 2018;74:69–79.
[20] Laguna R, Geremias N, Mauiri D, Alfonso J, Chiruzzo L, Ezzatti P, et al. 2020 IEEE PES Transm Distrib Conf Exhib - Lat Am T D LA 2020;2020:8–13.
[21] Jiménez AA, Gómez Muñoz CQ, García Márquez FP. Energ (Basel) 2018;11:1–16.
[22] Huang CG, Huang HZ, Li YF. IEEE Trans Ind Electron 2019;66:8792–802.
[23] Chen Z, Wu M, Zhao R, Guretno F, Yan R, Li X. IEEE Trans Ind Electron 2021;68: 2521–31.
[24] Xu Q, Chen Z, Wu K, Wang C, Wu M, Li X. IEEE Trans Ind Electron 2021;69: 2022–32.
[25] Guo J, Wang Z, Li H, Yang Y, Huang CG, Yazdi M, et al. Reliab Eng Syst Saf 2024; 245.
[26] Wang L, Guo W, Guo J, Zheng S, Wang Z, Kang HS, et al. Reliab Eng Syst Saf 2025; 255.
[27] Lin Y, Xiao M, Liu H, Li Z, Zhou S, Xu X, et al. Meas (Lond) 2022;192:110913.
[28] Yao Y, Wang N. Mech Syst Signal Process 2020;142:106772.

[29] Fang Q, Xiong G, Shang X, Liu S, Hu B, Shen Z. IEEE Int Conf Autom Sci Eng 2020-Augus 2020:588–93.
[30] Lin YH, Li GH. IEEE Trans Ind Inform 2022;18:7274–84.
[31] Gao Y, Wen Y, Wu J. IEEE Trans Neural Netw Learn Syst 2021;32:117–27.
[32] Hervé de Beaulieu M, Jha MS, Garnier H, Cerbah F. Reliab Eng Syst Saf 2024;252.
[33] Liao X, Chen S, Wen P, Zhao S. Adv Eng Inform 2023;58.
[34] Yang S, Tang B, Wang W, Yang Q, Hu C. Reliab Eng Syst Saf 2024;242.
[35] Pan L, Li G, Zhu T, Liu D, Wang Y, Lu Y. J Comput Inf Sci Eng 2025;25.
[36] Natl Renew Energy Lab 2022;V3(0):0.
[37] Larrosa NO, Akid R, Ainsworth RA. Int Mater Rev 2018;63:283–308.
[38] Jiang Z. Renew Sustain Energy Rev 2025;212.
[39] Wang L, Kolios A, Liu X, Venetsanos D, Rui C. Renew Sustain Energy Rev 2022;161.
[40] Drvoderic M, Pletz M, Schuecker C. J Compos Sci 2022;6.
[41] Suzuki T, Mahfuz H, Takanashi M. Int J Fatigue 2019;119:220–8.
[42] Xu Z, Li C, Yang Y. Appl Soft Comput J 2020;95.
[43] Xu Z, Bashir M, Liu Q, Miao Z, Wang X, Wang J, et al. Comput Ind Eng 2023;176.
[44] Dragomiretskiy K, Zosso D. IEEE Trans Signal Process 2014;62:531–44.
[45] Lin YH, Chang L, Guan LX. Reliab Eng Syst Saf 2024;248.
[46] Xu Q, Chen Z, Wu K, Wang C, Wu M, Li X. IEEE Trans Ind Electron 2021;69:2022–32.
[47] Rogers TJ, Gardner P, Dervilis N, Worden K, Maguire AE, Papatheou E, et al. Renew Energy 2020;148:1124–36.
[48] Gal Y, Ghahramani Z. 33rd International Conference on Machine Learning, 2016. ICML; 2016. p. 1661–80.
[49] Xu Z-F, Miao W-P, Li C, Jin J-T, Li S-J. Wuli Xuebao/Acta Phys Sin 2020;69.
[50] Jabbar A, Jianjun H, Jabbar MK, ur Rehman K, Bilal A. Sci Rep 2025;15.
[51] Zhang W, Guo Y, Jin Q. Symmetry (Basel) 2023;15.
[52] J. Kuria Kimotho, W. Sextro, An Approach for Feature Extraction and Selection from Non-Trending Data for Machinery Prognosis, n.d.
[53] Xu Z, Zhao K, Wang J, Bashir M. Adv Eng Inform 2024;62.
[54] E.B. Abrahamsen, T. Aven, F. Bouder, R. Flage, M. Ylönen, Z. Xu, , (2025).
[55] Taufik MH, Alkhalifah T. Artif Intell Geosci 2025;6.
[56] A. Kendall, Y. Gal, R. Cipolla, (2018).
[57] Xiang S, Qin Y, Zhu C, Wang Y, Chen H. ISA Trans 2020;106:343–54.
[58] Saidi L, Ben Ali J, Bechhoefer E, Benbouzid M. Appl Acoust 2017;120:1–8.
[59] Xu ZF, Yue MN, Li C. Wuli Xuebao/Acta Phys Sin 2019;68.
[60] Bashir M, Xu Z, Wang J, Guedes Soares C. J Mar Sci Eng 2022;10.